

Dichalcogenides and difulfides nanostructures for hydrogen storage

Flavio Bento de Oliveira and Andréia Luisa da Rosa*

Institute of Physics, Federal University of Goiás,

Campus Samambaia, 74690-900, Goiânia, Goiás, Brazil.

Abstract

Large-surface-area, two-dimensional (2D) layered materials are expected to have an advantage in hydrogen storage applications. Among a large number of 2D materials, monolayer dichalcogenides have emerged as promising candidate for hydrogen clean energy. In this work we investigate MoS_2 , porous MoS_2 and XS_2 as alternative materials for hydrogen storage. In this work we have investigated porous MoS_2 and XS_2 ($\text{X} = \text{Pd}, \text{Ni}$ and Pt) as alternative materials for hydrogen storage. Nickel selenide appears as a viable candidate for hydrogen storage, boasting a gravimetrics of 6.87%. We also show that MoS_2 nanopores could enhance the gravimetry for hydrogen storage. This enhancement occurs through the adsorption of H_2 molecules within the pore. Finally, AIMD calculations suggested that the structures identified in this work could be stable even at room temperature.

* andreialuisa@ufg.br

I. Introduction

The demand for energy development has continually increased, and therefore energy consumption is constantly increasing, causing global warming through the emission of pollutants into the atmosphere, leading to a probable future shortage of fossil fuels. With this there is a growing demand for renewable energy, with a growth rate per year of 14.7% [1]. Hydrogen is a potential energy carrier since its origin may come from clean sources. Nevertheless, storing hydrogen at densities greater than its natural density poses a challenge. There are four main methods for hydrogen storage: compression, liquefaction, metal hydrides and physisorption. The primary challenge lies in developing lightweight hydrogen storage materials at reasonable costs. Hydrogen boasts three times more energy value compared to fossil fuels [1]. Nevertheless, storing 1 kg of hydrogen requires approximately 11 m³ at ambient temperature, necessitating the storage of hydrogen fuel in cylinders with pressures ranging from 20 MPa to 80 MPa [2, 3]. This method is referred to as compression. Another approach is liquefaction, which involves cooling hydrogen down to 33.2 K. While hydrogen can be stored in open systems using this method, the evaporation and consumption of hydrogen are high and limited. The fuel is consumed in a very short time, limiting its application to specific cases, such as aircrafts [4, 5]. The currently used hydrogen storage in the industry is either metallic or in form of complex hydrides. However these hydrides cannot resolve the high pressure condition, and contain a large volume to be stored. Besides storage, another problem when using these hydrides is the fact that after a few cycles the metals used end up degrading or becoming brittle. Another problem often associated is the thermodynamics of metal hydrides reactions, the large amount of heat generated during refuelling, thus making it difficult to store hydrogen.

It is estimated that storing hydrogen requires a weight (wt) between 4 wt% to 7 wt% of hydrogen [6–8]. This has led to the search for new technologies. In the search for new materials, two-dimensional nanostructures have gained interest following the discovery

of graphene, whose properties differed significantly from those of its three-dimensional counterpart, graphite [9]. These materials exhibit electrical properties highly appealing for technological applications and hold promise for reducing the dimensions of currently produced electronic devices. This has led to a growing interest in exploration of other two-dimensional materials, in particular for hydrogen storage [3, 10, 11]. It is expected that large-surface-area, two-dimensional (2D) layered materials have an advantage in hydrogen storage applications. Therefore, finding materials that can effectively contain hydrogen is crucial for the application of hydrogen energy.

MX_2 ($\text{M} = \text{Mo}, \text{W}$ and $\text{X} = \text{S}, \text{Se}, \text{Te}$) have several polytypes the 2H (2H- MoS_2) has semiconductor behavior and 1T(1T- MoS_2) or 1T'(1T'- MoS_2) both metallic phase. It has been suggested that the performance of the layered material has a dependence with the structural phase [12]. For example, MoS_2 nanotubes showed 1.2 % wt hydrogen storage capacity. The authors attributed these results to the high specific surface area of MoS_2 nanotubes [10]. Another usual approach for improving hydrogen storage capacity is doping. Hydrogen storage performances of pure MoS_2 monolayer and the one decorated with 3d and 4d atoms were studied via the first-principles DFT calculations [13, 14]. Storage capacity of around 6 wt%. [13] has been achieved. Although doping is a possible route to enhance adsorption energies on MoS_2 , doping has proven to be difficult in low-dimensional materials [15, 16]. Previous investigations on hydrogen intercalation in MoS_2 bilayers [17] has suggested that the insertion energies of hydrogen molecules as a function of hydrogen concentration in MoS_2 can be accommodated in MoS_2 bilayers without a major change in the interlayer spacing.

Previous work on hydrogen intercalation in MoS_2 bilayers [17]. The insertion energies of hydrogen molecules as a function of hydrogen concentration in MoS_2 have shown that at a reasonable number of H_2 molecules can be accommodated in MoS_2 bilayers without a major change in the interlayer spacing. Hydrogen can be liquified at ambient pressure at a temperature of -253°C , which increases its density to about 70 kg /m^3 , facilitating

transportation of smaller volumes. Recently, bulk and exfoliated MoS₂ were used to understand hydrogen storage potential of the bulk and exfoliated MoS₂ was addressed under 1-9 bar hydrogen pressure. After the absorption process. The bulk and exfoliated MoS₂ stored 220 and 450 sccm hydrogen, respectively. Besides, the weight percent hydrogen storage was determined to be 1.2 and 2.4 wt%, respectively[18].

On the other hand similar layered structures of formed by Pd, Ni and Pt TMDs remained largely unexplored with few publications focusing on their electronic, mechanical, optical and thermoelectric properties of monolayer PdS₂ and PdSe₂ [19–21]. These structures show a different reactivity than their MoS₂ counterparts and therefore could lead to other weight percent hydrogen.

In this work we investigate MoS₂, porous MoS₂ and XS₂ as alternative materials for hydrogen storage. In this work we have investigated porous MoS₂ and XS₂ (X = Pd, Ni and Pt) as alternative materials for hydrogen storage. Nickel selenide appears as a viable candidate for hydrogen storage, boasting a gravimetrics of 6.87%. We also show that MoS₂ nanopores could enhance the gravimetry for hydrogen storage. This enhancement occurs through the adsorption of H₂ molecules within the pore. Our AIMD calculations suggests that the structures identified in this work could be stable even at room temperature.

II. Computational Details

In this work, we compute electronic and atomic properties using VASP (Vienna Ab-initio Simulation Package) computational code [22, 23]. The calculations presented here have 400 eV. We use the PAW[24] method together with the exchange-correlation functional in the PBE to describe the electronic interactions [25]. The criteria used for the convergence of energy was 10⁻⁴eV. AIMD calculations have been performed using the Andersen thermostat at 300K. Time steps of for a total simulation time of 5 ps. The NEB method is used to determine the path which a atom on the crystal energy surface would take when connected by two states, which are minimum energy states of the system. NEB will seek

for the lowest energy cost path between two states. The path through the potential energy surface show us the energy barrier which the atom needs to overcome to go to a minimum energy state to another minimum energy state.

III. Monolayers and nanopores of MoX_2

The most stable structure among the MoS_2 polytypes is 2H at ambient conditions. Meanwhile, other polytypes of MX_2 , including 1T- MoS_2 and 1T'- MoS_2 have been found [26–28]. These structures are metallic materials, while the 2H- MoS_2 structure exhibits semiconductor properties.

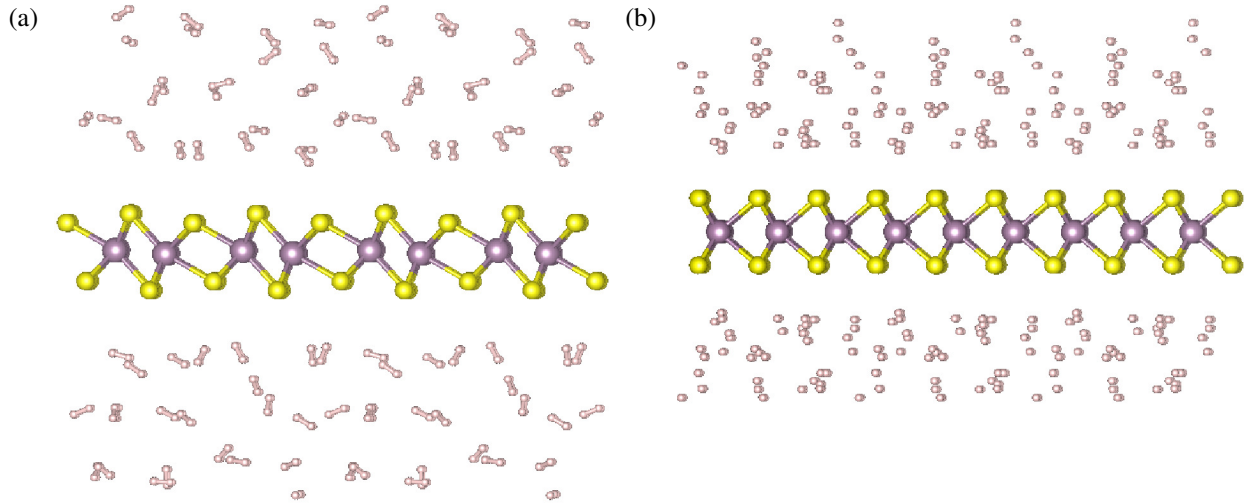


FIG. 1: 48 H_2 molecules adsorbed on a) 1T'- MoS_2 structure and b) the 2H- MoS_2 structure.

Gravimetric analysis is a quantitative analytical technique that enables the determination of the amount of a substance in a given mixture, thus the gravimetric hydrogen storage capacity for 2H- MoS_2 reached 6.97wt%, it was seen that the hydrogen molecules are inert on the 2H- MX_2 layer, being more energetically favorable the molecule perpendicular to the structures with type 2H- MX_2 , molybdenum disulfide (MoS_2) demonstrates a structure with higher storage capacity in relation to other transition metal dichalcogenides. Adsorption energy of around 200 meV as shown in Fig. 2, for the 2H lies in the physisorption range.

For the 1T' we see formation of bonds between hydrogen and the surface atoms.

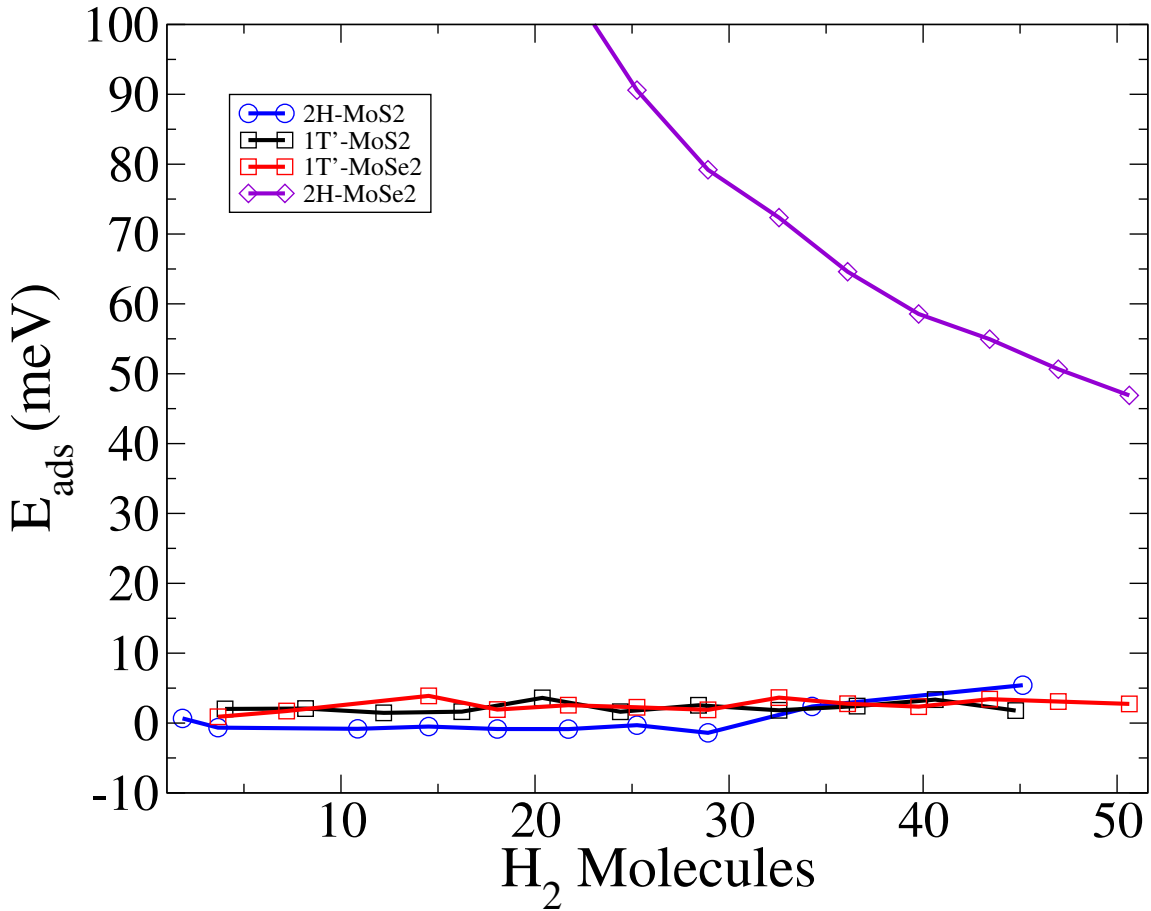


FIG. 2: Adsorption energy of H₂ molecules on 1T' and 2H phases of MoS₂ and MoSe₂ as a function of number of hydrogen molecules.

In order to find a new route for hydrogen storage, defective 2H-MoS₂ was investigated. In our previous work we have investigated several point defects [29, 30]. The most common defects in MoS₂ are S and Mo vacancies. Beyond spontaneous defects, ion beam irradiation can also be used to promote larger defects [?] so we calculated the 2H-MoS₂ in vacancy defects in order to understand the behavior of hydrogen molecules in the presence of these defects, as shown in the Fig. 3.

In order to estimate the possibility of additional H₂ molecules within the nanopores, the

reaction of H_2 molecules was investigated. We have performed NEB [31, 32] calculations to estimate the potential barrier for the molecule to diffuse through the pore. The NEB was performed along a path perpendicular to the MoS_2 plane. The intermediate states are shown in Fig. 4. Five images were chosen along the diffusion path. Along the chosen path a barrier of 0.35 eV is found, as shown in Fig. 4. This implies that additional molecules could reside within the pore, thus enhancing the storage capacity of 2H- MoS_2 .

The gravimetric storage of H_2 adsorbed on the defective layers containing one vacancy results in 7.09 wt%. Defect engineering could be a path for increasing hydrogen storage capacity.

IV. Intercalation of H_2 in bilayers of MoS_2

Effective approaches to fabricate bandgap engineered bilayer MoS_2 structures, an important step to fabricate homo/hetero-structures, and thus advanced electronic devices have been recently developed [33, 34]. This is specially interesting for energy storage applications, since molecules can be trapped between the layers. We now discuss hydrogen intercalation in MX_2 bilayers. The relaxed configurations are shown in Fig. 5. We calculated the gravimetric hydrogen storage capacity for the 2H- MoS_2 and 1T'- MoS_2 bilayers respectively. The gravimetric hydrogen storage varied from 3.39 wt% and 2.17wt%, as shown in Tab. I. We analyzed the adsorption energy of the 2H-bilayer and 1T'-bilayer as a function of the H_2 numbers. The results are shown in Fig. 6

V. Molecular dynamics of H_2 adsorbed on MoS_2

In order to investigate temperature effects of adsorption of H_2 on both polytypes, 1T'- MoS_2 and 2H- MoS_2 MD simulations were performed at a temperature of 300 K with the Andersen thermostat bath in contact with the system. The RDF revealed that for the 2H phase, the equidistances equivalent to the first and second neighbors of a referential Mo, are illustrated in Ref. 8. Additionally, the structure of 2H- MoS_2 did not show structural distortion.

structure	ML wt%	BL 2H(1T') wt%
1T'(2H)-MoS ₂	6.43(6.97)	3.39(2.17)
MoS ₂ -V _{2S}	7.09	-
MoS ₂ -V _{1Mo}	7.11	-
MoS ₂ -V _{1Mo4S}	7.13	-
MoS ₂ -V _{1Mo6S}	7.14	-
MoS ₂ -V _{3Mo2S}	7.52	-
1T'(2H)-MoSe ₂	4.67(5.22)	1.55 (1.55)
WS ₂	4.66 (4.66)	1.60 (1.60)
WSe ₂	3.42 (3.42)	0.92 (0.92)
MoTe ₂	3.34 (3.34)	1.13 (1.13)
WTe ₂	2.66 (2.66)	0.91 (0.91)

TABLE I: Hydrogen storage capacity, where the MX₂(M=Mo,W and X=S,Se,Te). Note that for vacancies, additional H₂ storage capacity is considered within the nanopore.

On the other hand, for 1T'-MoS₂, owned to the asymmetry between the S-Mo-S bonds, additional peaks were seen, as depicted in Fig. 9(b).

VI. MoX₂ (X= Pd, Pt and Ni)

Next we investigate XY₂ nanostructures, namely (X = Ni,Pt,Pd) and (Y = S, Se) in 1T and 2H polytypes. First we discuss the thermodynamic stability of pristine structures. We find that the dichalcogenides, 1T-NiS₂, 1T-PtS₂, and 1T-PdS₂ are higher in energy compared to their respective 2H polytypes (2H-NiS₂, 2H-PtS₂, and 2H-PdS₂). The lattice parameters for 1T-NiS₂, 1T-PtS₂, and 1T-PdS₂ are 3.35 Å, 3.54 Å, and 3.56 Å, respectively. In the 2H polytype, 2H-NiS₂ has a lattice parameter of 3.54 Å, 2H-PtS₂ has 3.48 Å, and 2H-PdS₂ has 3.92 Å, as shown in Figs. 10(a)-(c). For diselenides, a similar trend is found for NiSe₂, PdSe₂, and PtSe₂. The 1T polytypes show higher thermodynamic stability with lattice parameters of 3.53 Å, 3.74 Å, and 3.75 Å, respectively, compared to the 2H polytypes with lattice parameters of 3.56 Å, 4.01 Å, and 3.63 Å, as depicted in Figs. 10(d)-(e).

Adsorption energy for a single molecule on III. It was found that due to the low

NiS ₂								
site	1T				2H			
	E _{ads} (meV)	d _{H-S} (Å)	d _{H-S₂} (Å)	d _{H-X} (Å)	E _{ads} (meV)	d _{H-S} (Å)	d _{H-Se} (Å)	d _{H-X} (Å)
Top bridge	30(30)	2.86(3.24)		3.90(4.14)	-0.64(-0.63)	2.62(2.94)	4.62(4.51)	
Top hollow	70(70)	2.98(3.22)		3.92(4.27)	-0.65(-0.62)	3.11(2.97)	3.96(3.98)	
Top X	60(60)	2.98(3.37)		3.38(3.83)	-0.66(-0.64)	3.11(3.10)	3.41(3.62)	
Top S	20(20)	2.92(3.30)		4.51(4.87)	-0.65(-0.64)	2.94(3.01)	4.52(4.33)	
Bottom bridge	30(30)		3.15(3.14)	3.95(4.14)	-0.64(-0.62)		2.62(2.88)	3.57(3.78)
Bottom X	30(30)		5.75(3.05)	4.26(3.7)	-0.65(-0.62)		3.14(2.96)	3.96(3.97)
Bottom S	60(60)		2.95(3.16)	3.40(4.34)	-0.65(-0.63)		3.13(3.05)	3.40(3.61)
Bottom hollow	30(30)		4.35(3.12)	4.38(4.61)	-0.65(-0.66)		2.71(3.55)	4.31(4.92)

TABLE II: Adsorption energy and atomic distances of the material NiS₂. in brackets for H_2 molecule perpendicular to the monolayer and without brackets parallel to the monolayer, note disordered refer to a structural disorder.

concentration of H_2 in the network, it caused the dissociation of H_2 on PdS₂ and PtS₂, forming S-H bonds. When compared to adsorption at high concentrations of H_2 , the adsorption energy shows a dependency on the concentration. As the concentration of H_2 increases, the available adsorption sites on the surface become unavailable. As all surface sites become occupied, the addition of further H_2 molecules does not lead to a significant decrease in adsorption energy.

The adsorption energy of the investigated structures reached the order of 100 meV. A close-up view of the region with high H_2 concentration reveals that as the H_2 concentration increases, the available adsorption sites on the surface become saturated, forming layers of H_2 as shown in Fig. 6.

For 1T-NiS₂, it was seen that for a quantity of H_2 adsorption molecules higher than 28 molecules, the nickel disulfide (NiS₂) structure exhibits structural disorder caused by the absorption of H_2 , forming S-H bonds as demonstrated in Fig. 14. A storage capacity of 10.8 wt% was obtained. Alternatively, considering the quantity of 28 H_2 molecules, the gravimetry is 8.83 wt%. Calculations show that for 2H-NiS₂, the gravimetric value is 11.44

wt%, and there is no significant structural distortion.

For 1T-PdS₂, a similar behavior was obtained from 28 H₂ molecules. This result is independent on the molecule orientation. A storage capacity of 8.04 wt% is found with a small amount of H₂ dissociating on the surface sulphur atoms (0.3%). Due to larger weight of Pd compared to Ni, 2H-PdS₂ was found to have a storage capacity of 8.53 wt%.

It was found that for the 1T-PtS₂ polytype, the H₂ adsorption behavior was similar to 1T-PdS₂. However, due to the fact that Pt is heavier than Pd, the storage capacity of 1T-PtS₂ was 5.45 wt%, whereas for 2H-PtS₂, it was found to be 5.79 wt%, as shown in Tab. IV.

Adsorption on dichalcogenides resulted in the dissociation of H₂ and a modification of the structure, leading to structural changes. Nonetheless, when compared with the 1T-NiS₂ structures, an increase in storage capacity from 8.61 wt% to up to 11.44 wt% was found. Therefore, both NiS₂ polytypes and PdS₂ polytypes can be considered promising candidates for hydrogen storage.

VII. Conclusions

In this work we have investigated porous MoS₂ and XS₂ (X = Pd, Ni and Pt) as alternative materials for hydrogen storage. Nickel selenide appears as a viable candidate for hydrogen storage, boasting a gravimetry of 6.87% wt. We also show that MoS₂ nanopores could enhance the gravimetry for hydrogen storage. This enhancement occurs through the adsorption of H₂ molecules within the pore. AIMD suggested that the structures identified in this work could be stable even at room temperature.

-
- [1] *Statistical Review of World Energy* (2023).
 - [2] L. Schlapbach and A. Züttel, *Nature* **414**, 353 (2001).
 - [3] A. Züttel, *Naturwissenschaften* **91**, 157–172 (2004).
 - [4] L. Zhou, *Renewable and Sustainable Energy Reviews* **9**, 395 (2005).

- [5] C. Tarhan and M. A. Çil, *Journal of Energy Storage* **40**, 102676 (2021).
- [6] J. Graetz, *Chem. Soc. Rev.* **38**, 73 (2009).
- [7] S. Lynch, in *Stress Corrosion Cracking*, Woodhead Publishing Series in Metals and Surface Engineering, edited by V. Raja and T. Shoji (Woodhead Publishing, 2011) pp. 90–130.
- [8] Y. Cao, *ACS Nano* **15**, 11014 (2021).
- [9] A. K. Geim and K. S. Novoselov, *Nature Materials* **6**, 183 (2007).
- [10] J. Chen and Kuriyama, *J. Am. Chem. Soc.* (2001).
- [11] Y. H. T. H. S. T. Chen J, Kuriyama N, *J Am Chem Soc.* **123**, 11813 (2001).
- [12] J. Chen, J. Cao, J. Zhou, Y. Zhang, M. Li, W. Wang, J. Liu, and X. Liu, *Phys. Chem. Chem. Phys.* **22**, 430 (2020).
- [13] S. Yang, X. Wang, G. Lei, H. Xu, Z. Wang, J. Xiong, and H. Gu, *Surfaces and Interfaces* **26**, 101329 (2021).
- [14] S. Yang, Y. Liu, G. Lei, Y. Xie, L. Peng, H. Xu, Z. Wang, and H. Gu, *International Journal of Hydrogen Energy* **46**, 24233 (2021).
- [15] V. P. Pham and G. Y. Yeom, *Advanced Materials* **28**, 9024 (2016).
- [16] E. S. O. M. e. a. Altuntepe, A., *J Mater Sci: Mater Electron* **35**, 69 (2024).
- [17] Z. Zhu, H. Peelaers, and C. G. Van de Walle, *Phys. Rev. B* **94**, 085426 (2016).
- [18] A. Altuntepe, S. Erkan, M. A. Olğar, S. Çelik, and R. Zan, *International Journal of Hydrogen Energy* **56**, 690 (2024).
- [19] E. A. Moujaes and W. Diery, *Physica E: Low-dimensional systems and nanostructures* **128**, 114611 (2021).
- [20] S. Deng, L. Li, and Y. Zhang, *ACS Applied Nano Materials* **1** (2018), 10.1021/acsanm.8b00363.
- [21] Y. Z. G. J. e. a. Zhao, X.W., *Sci. Rep.* **10**, 4028 (2020).
- [22] G. Kresse and D. Joubert, *Phys. Rev. B* **59**, 1758 (1999).
- [23] G. Kresse and J. Furthmüller, *Computational Materials Science* **6**, 15 (1996).

- [24] P. E. Blöchl, Phys. Rev. B **50**, 17953 (1994).
- [25] K. E. M. Perdew, J. P.; Burke, Phys. Rev. Lett. **77**, 3865–3868 (1996).
- [26] W. Zhao, J. Pan, Y. Fang, X. Che, D. Wang, K. Bu, and F. Huang, Chemistry – A European Journal **24**, 15942 (2018).
- [27] F.-Q. Huang, W. Zhao, J. Pan, F. Yuqiang, X. Che, D. Wang, and K. Bu, Chemistry **24** (2018), 10.1002/chem.201801018.
- [28] W. J. W. L. e. a. Liu, L., Nature Mater. **17**, 1108–1114 (2018).
- [29] V. Onita, M. Kendjy, F. B. de Oliveira, and A. L. da Rosa, Brazilian Journal of Physics **54**, 7 (2023).
- [30] H.-P. Komsa and A. V. Krasheninnikov, Phys. Rev. B **91**, 125304 (2015).
- [31] G. Henkelman, B. P. Uberuaga, and H. Jónsson, The Journal of Chemical Physics **113**, 9901 (2000).
- [32] G. Henkelman and H. Jónsson, The Journal of Chemical Physics **113**, 9978 (2000).
- [33] W. Zhou, C. Yuan, A. Hong, X. Luo, and W. Lei, Nanoscale **10**, 1145 (2018).
- [34] X. W. W. H. e. a. Cheng, X., Front. Phys. **18**, 53303 (2023).

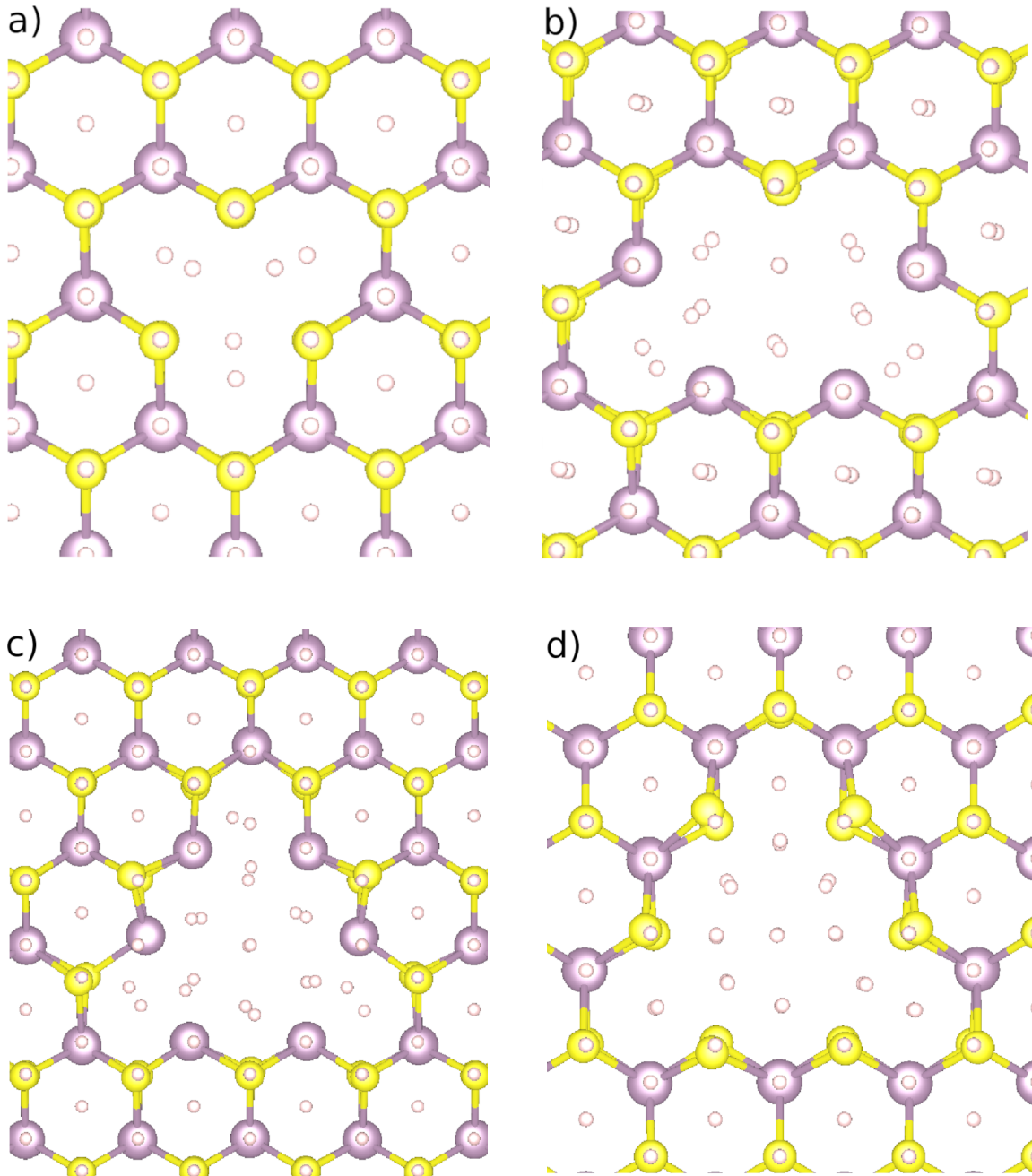


FIG. 3: Adsorbed hydrogen molecules on MoS₂ nanopores: a) molybdenum monovacancy, b) monovacancy of molybdenum and four sulfur vacancies, c) monovacancy of molybdenum and six sulfur vacancies and d) three vacancy of molybdenum and six sulfur vacancies.

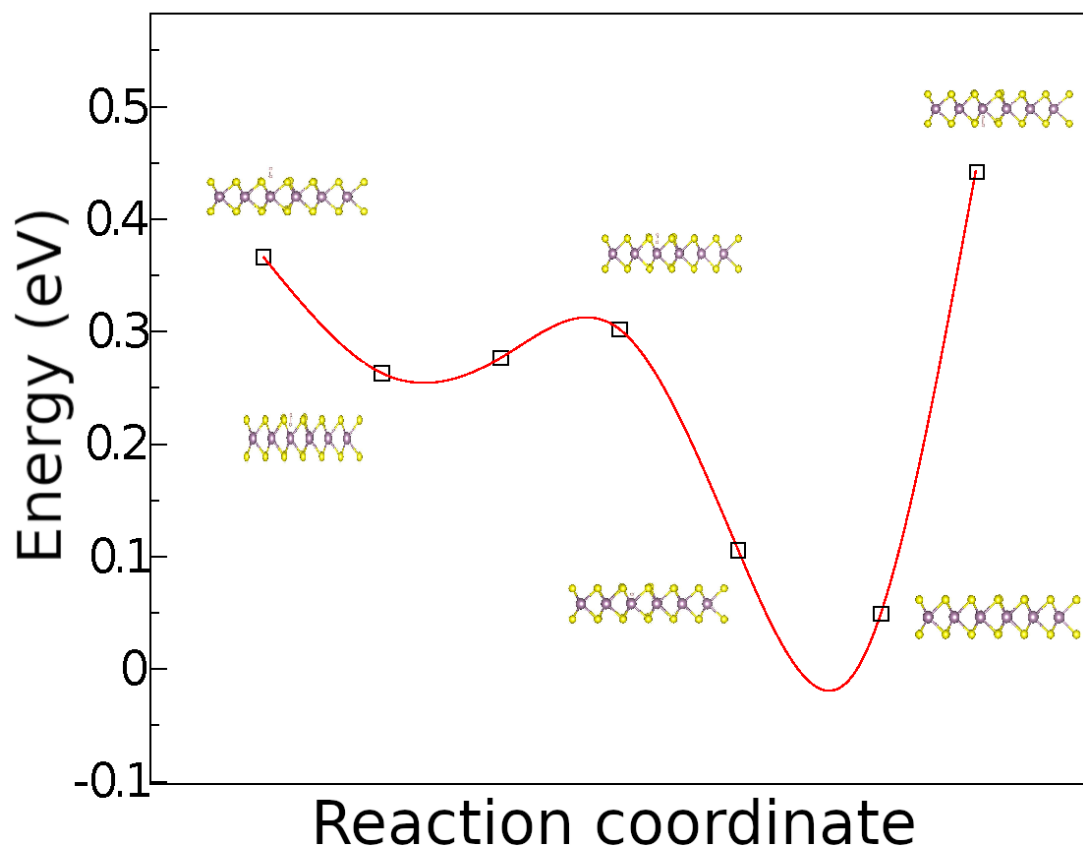


FIG. 4: Energy as a function of reaction coordinate, where a hydrogen molecule diffuses through the nanopore with a molybdenum vacancy.

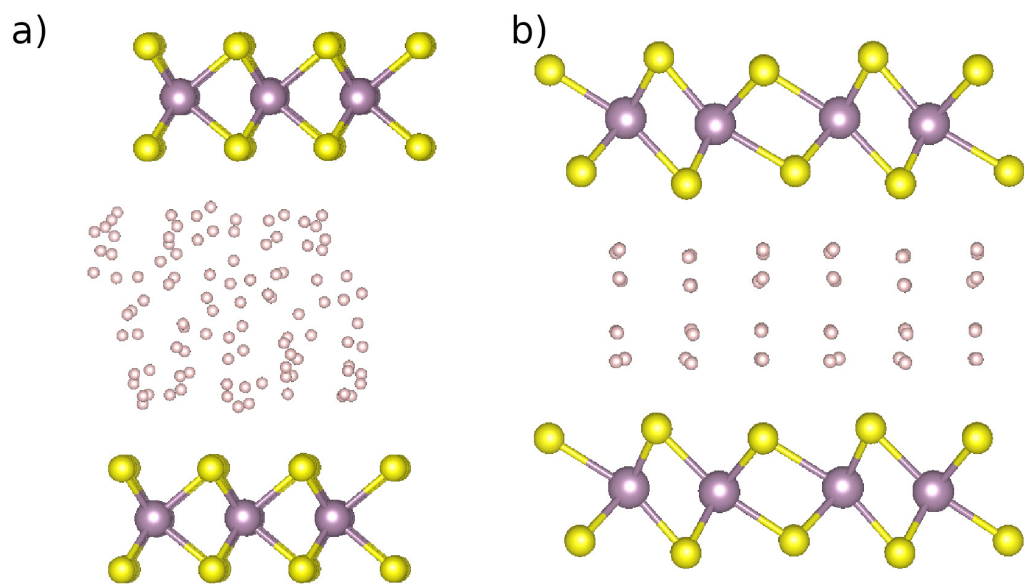


FIG. 5: Intercalated H_2 molecules in a) 2H-MoS₂ and b) 1T'-bilayers.

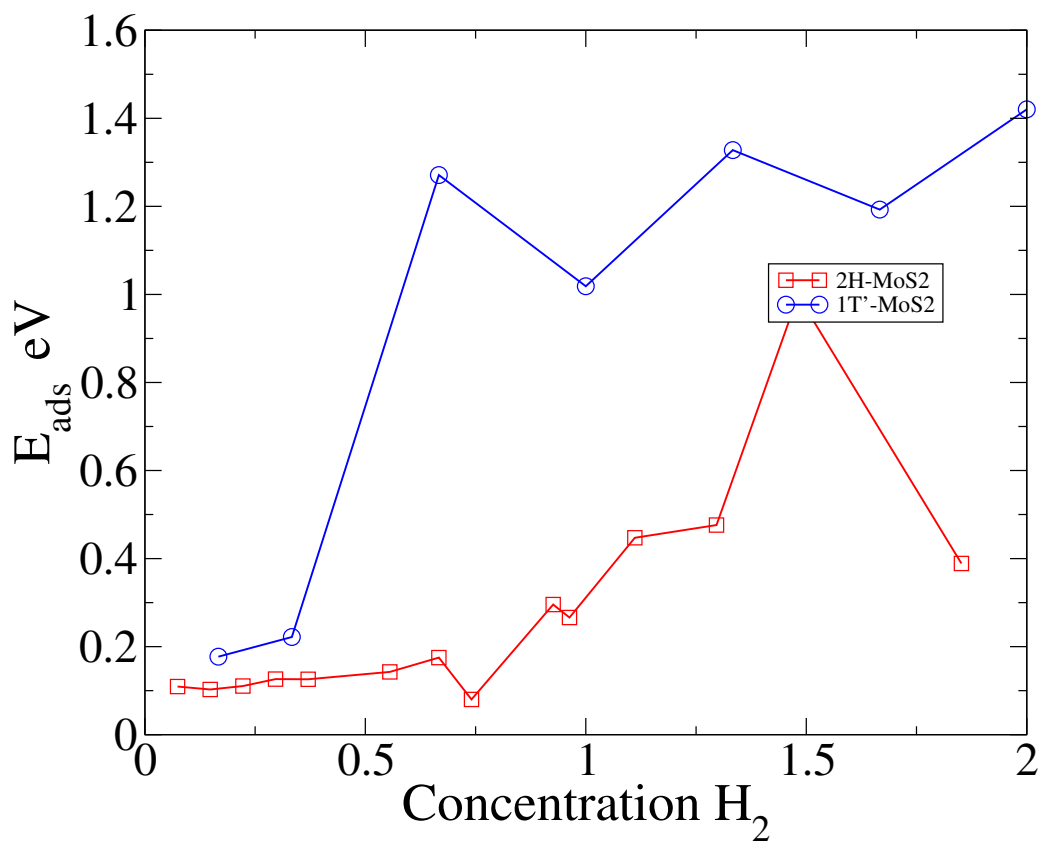
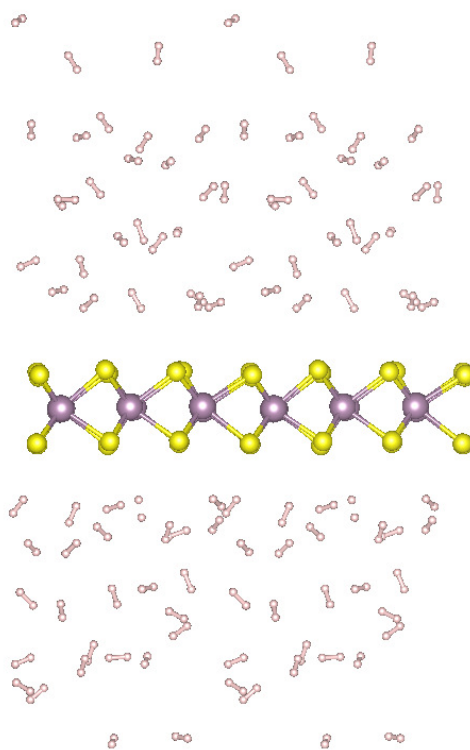


FIG. 6: Adsorption energy of hydrogen molecules for 1T' bilayer (blue) and 2H bilayer (red).

(a)



(b)

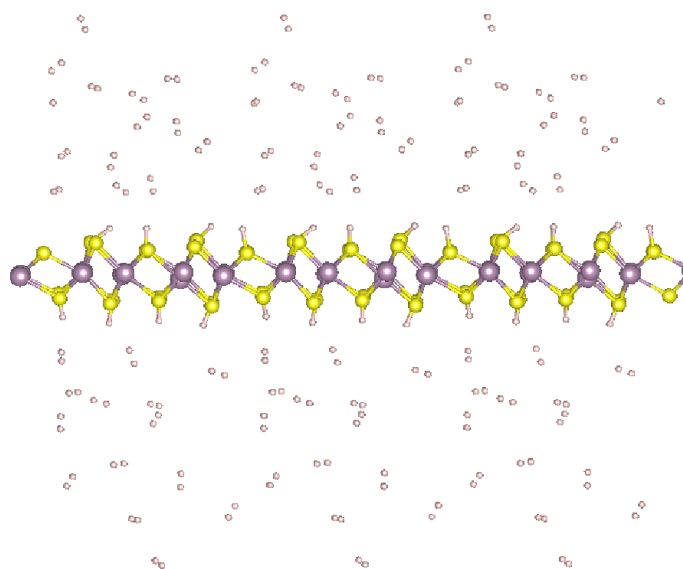


FIG. 7: Snapshots of AIMD simulations for 2H-MoS₂ and 1T' structure performed at 300K.

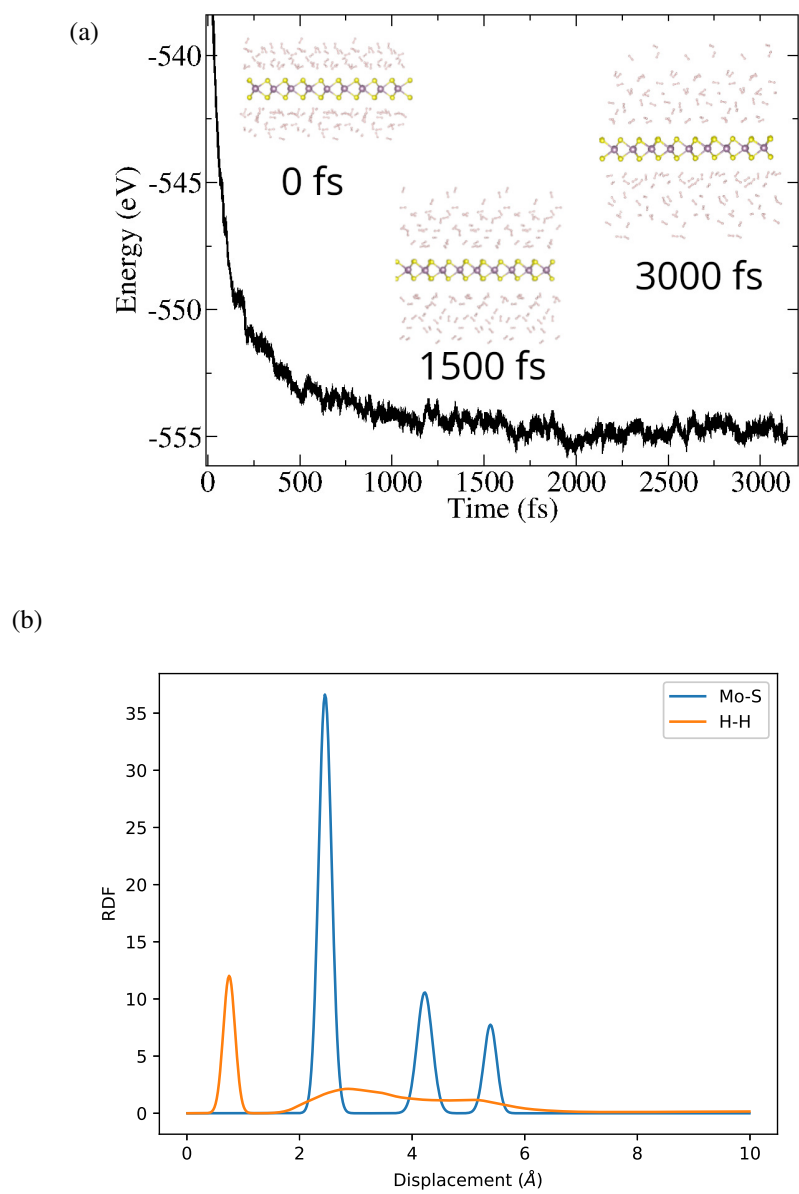


FIG. 8: Snapshots of AIMD simulations for 2H-MoS₂ at 300K.

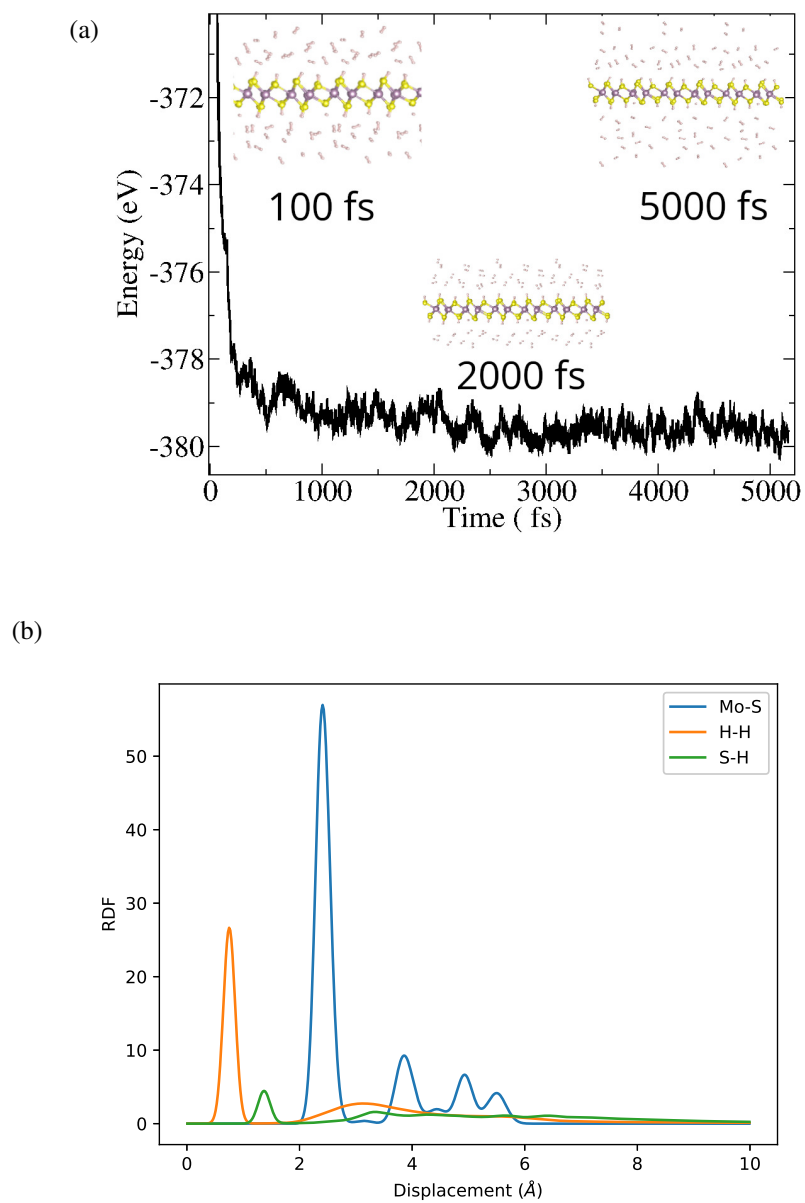


FIG. 9: AIMD simulations at 300K for 1T'-MoS₂. a) Energy as a function of time and b) RDF. Snapshots at 100, 2000 and 5000 fs simulation times are shown in the inset.

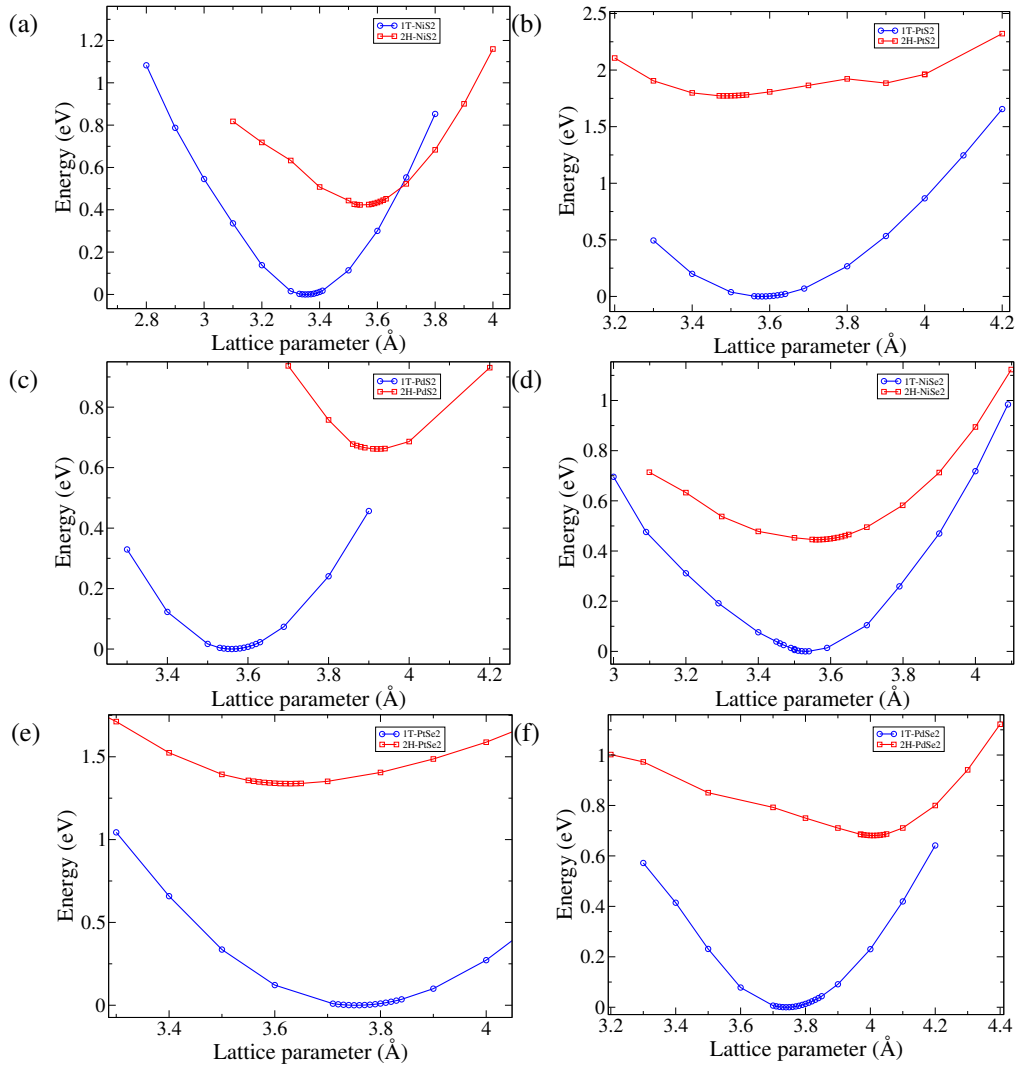


FIG. 10: Total energy as a function of lattice parameter for a) NiS_2 , b) PtS_2 , c) PdS_2 , d) NiSe_2 , e) PtSe_2 and f) PdSe_2 .

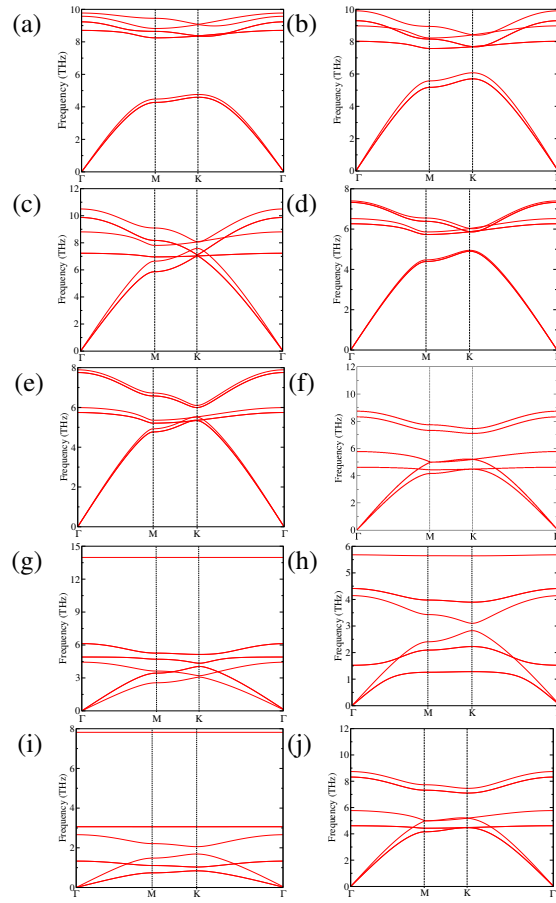


FIG. 11: Phonon dispersion for pristine a) 1T-PtS₂, b) 1T-PtdS₂, c) 1T-NidS₂, d) 1T-PtSe₂, e) 1T-PtdSe₂, f) 1T-NidSe₂, g) 2H-PtS₂, h) 2H-PdS₂, i) 2H-NiS₂, j) 2H-PtSe₂, k) 2H-PdSe₂ and l) 2H-NiSe₂.

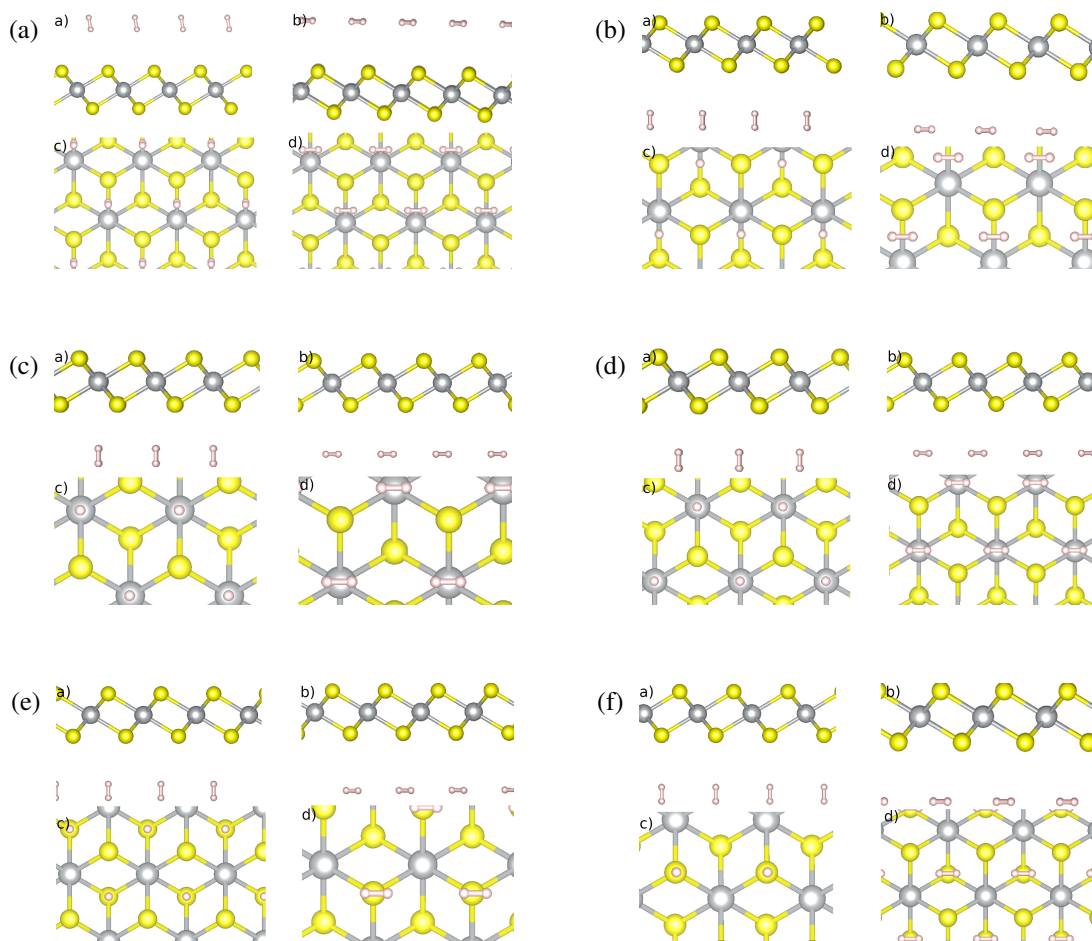


FIG. 12: Hydrogen adsorption on NiS₂ (clockwise) : a) bridge (side A), b) bridge (side B), c) top-X (side A), d) bottom-X (side B), e) hollow (side A) and f) bottom (side B). a) sideview with H₂ perpendicular to the layer, b) sideview with H₂ parallel to the layer, c) topview with H₂ perpendicular to the layer, d) topview with H₂ parallel to the layer.

NiSe ₂								
site	1T				2H			
	E _{ads} (meV)	d _{H-S} (Å)	d _{H-Se} (Å)	d _{H-X} (Å)	E _{ads} (meV)	d _{H-S} (Å)	d _{H-Se} (Å)	d _{H-X} (Å)
Top bridge	-0.57	3.05		4.09	dis.			
Top hollow	-0.56	3.33		4.38	-0.53	3.01		3.99
Top X	-0.53	3.03		3.47	-0.53	2.96		3.41
Top S	-0.57	2.90		4.62	dis.			
Bottom bridge	-0.57		3.38	4.24	dis.			
Bottom X	-0.57		3.52	4.58	-0.57		3.47	5.79
Bottom S	-0.57		3.38	3.94	-0.56		3.20	3.73
Bottom Se	-0.56		2.87	4.59	dis.			

PdSe ₂								
site	1T				2H			
	E _{ads} (meV)	d _{H-S} (Å)	d _{H-Se} (Å)	d _{H-X} (Å)	E _{ads} (meV)	d _{H-S} (Å)	d _{H-Se} (Å)	d _{H-X} (Å)
Top bridge	-0.57	3.10		4.16	dis.			
Top hollow	-0.52	2.99		4.05	-0.58	3.36		4.25
Top X	-0.53	3.02		5.05	-0.56	3.03		3.39
Top S	-0.57	2.88		4.71	dis.			
Bottom bridge	-0.57		3.39	4.27	dis.			
Bottom X	-0.52		3.02	4.04	-0.55		2.95	5.52
Bottom S	-0.57		3.39	3.90	-0.58		3.28	3.52
Bottom Se	-0.57		2.88	4.71	dis.			

PtSe ₂								
site	1T				2H			
	E _{ads} (meV)	d _{H-S} (Å)	d _{H-Se} (Å)	d _{H-dis.} (Å)	E _{ads} (meV)	d _{H-S} (Å)	d _{H-Se} (Å)	d _{H-X} (Å)
Top bridge 40	2.87		3.95	dis.				
Top hollow	20	3.50		4.62	20	3.06		4.99
Top dis.	50	3.13		3.53	10	3.90		4.78
Top S	20	3.02		4.84	dis.			
Bottom bridge	20		3.44	4.32	dis.			
Bottom dis.	20		3.43	4.52	20		3.64	6.12
Bottom S	20		3.57	4.15	diss.			
Bottom Se	20		2.99	4.81	dis.			

TABLE III: Adsorption energy and interatomic distances for NiSe₂, PdSe₂ and PtSe₂. H₂ molecule perpendicular (parallel) to the monolayer. Disordered refers to a structural disorder.

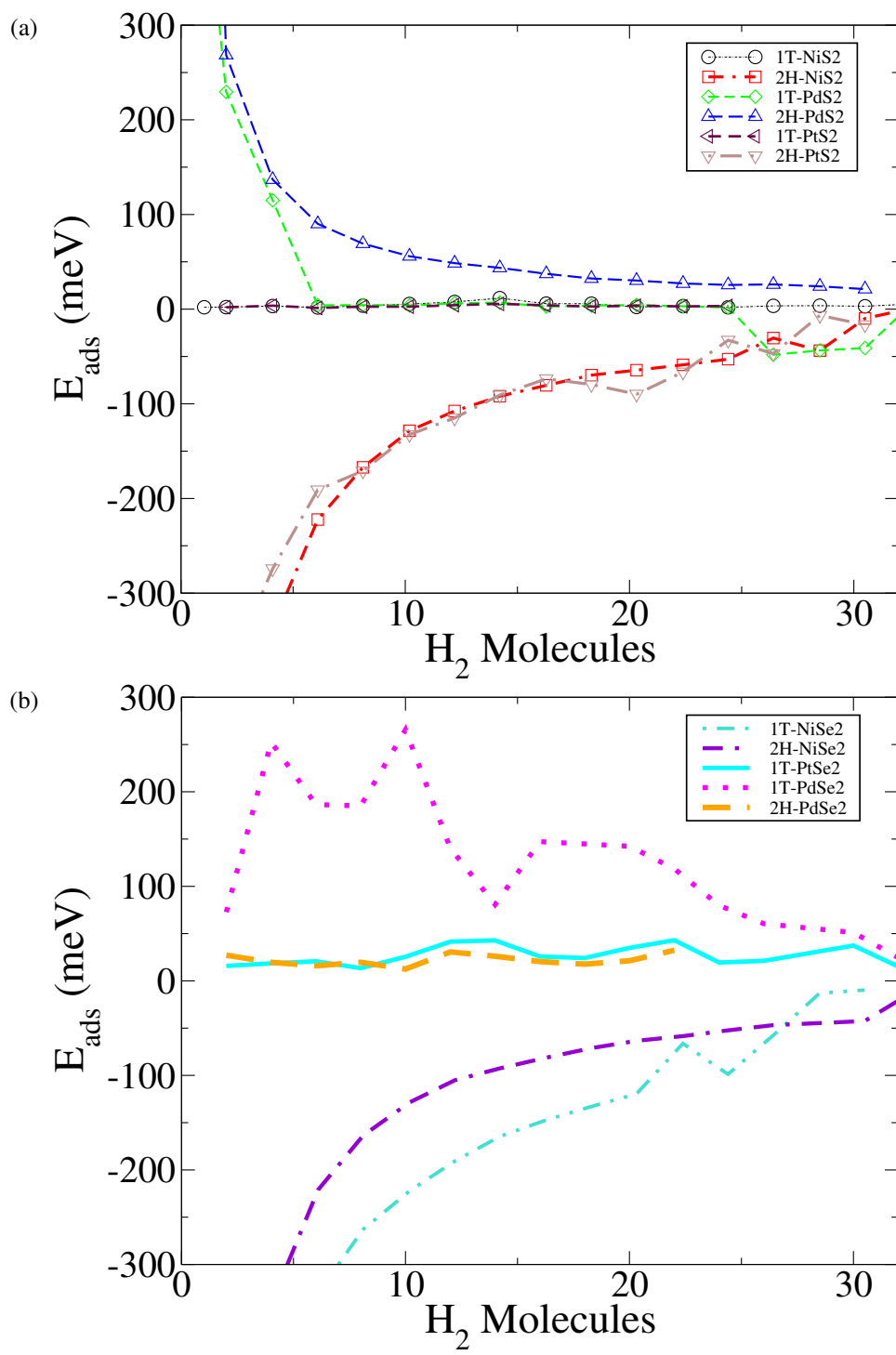


FIG. 13: Adsorption energy E_{ads} of H_2 for MS_2 as a function of the number of H_2 molecules.

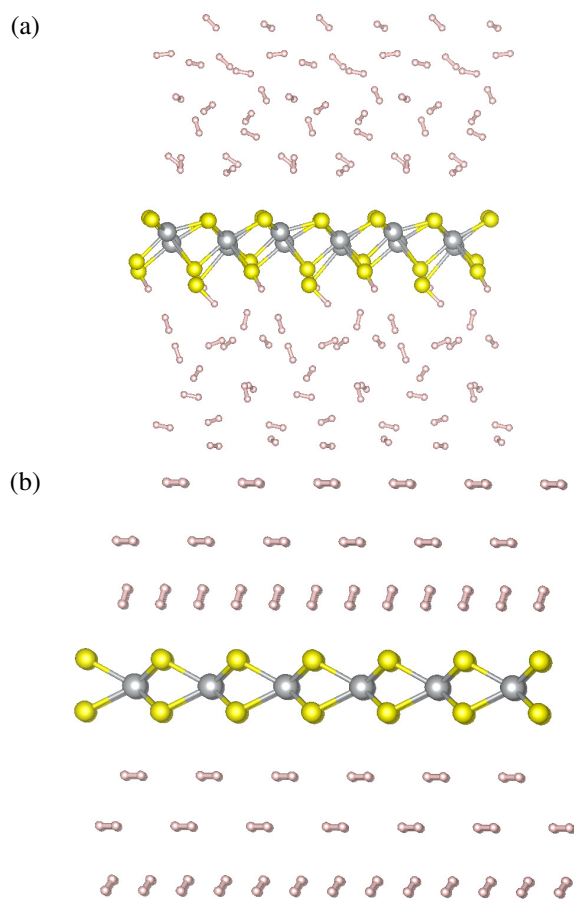


FIG. 14: a) Adsorption of 32 molecules on a) 1T-NiS₂ structure and b) 2H-NiS₂ structure.

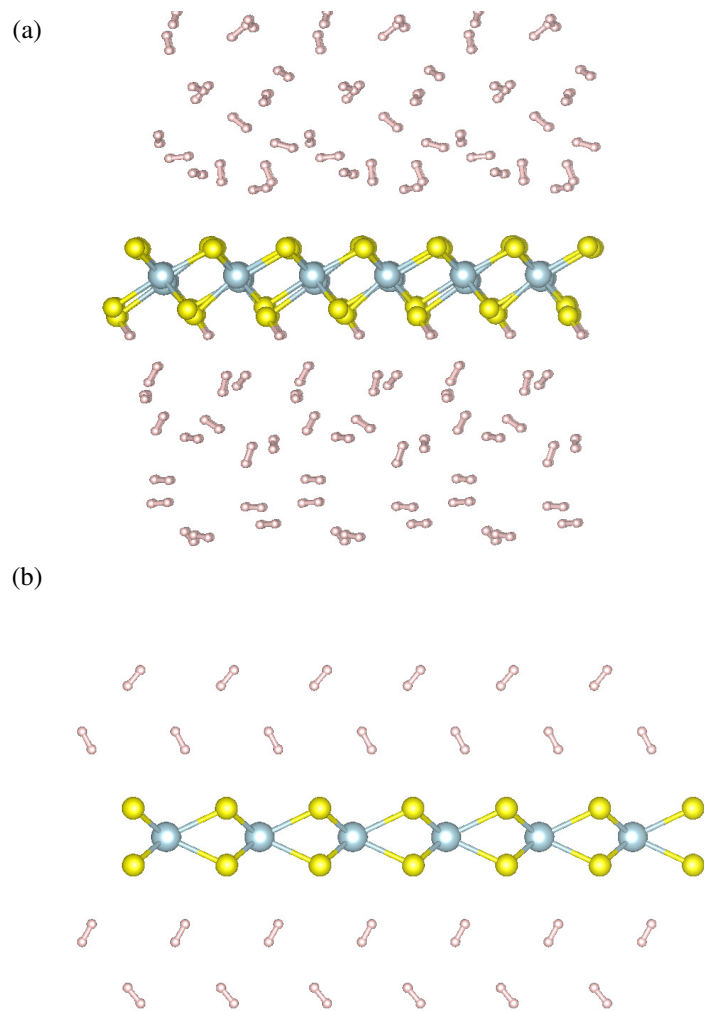


FIG. 15: Adsorption of 32 H_2 molecules on a) 1T- PdS_2 and b) 2H- PdS_2 .

	Gravimetry (wt%) E_{ads} (meV)	
1T-NiS ₂	10.8	30
2H-NiS ₂	11.44	10
1T-PtS ₂	5.45	30
2H-PtS ₂	5.79	-160
1T-PdS ₂	8.04	20
2H-PdS ₂	8.53	210
1T-NiSe ₂	6.87	-110
2H-NiSe ₂	6.87	-130
1T-PtSe ₂	4.33	15
2H-PtSe ₂	3.28	27
1T-PdSe ₂	5.71	24
2H-PdSe ₂	3.99	32

TABLE IV: Gravimetric analysis for disulphides and diselenides for H₂ adsorption at maximum hydrogen concentration for each structure.